Stability and Stationary Response of a Skew Jeffcott Rotor with Geometric Uncertainty

Nicolas Driot, Alain Berlioz, Claude-Henri Lamarque

Stability and Stationary Response of a Skew Jeffcott Rotor With Geometric Uncertainty

Nicolas Driot
LaMCoS, CNRS UMR 5259, INSA-Lyon, Université de Lyon, 20, rue des Sciences, F69621 Villeurbanne Cedex, France

Alain Berlioz
LGMT, INSA, UPS, Université de Toulouse, 135, Avenue de Rangueil, F 31077 Toulouse, France

Claude-Henri Lamarque
DGCB, URA CNRS 1652, ENTPE, Université de Lyon, 3, rue Maurice Audin, F 69518 Vaulx-en-Velin, France

The aim of this work is to apply stochastic methods to investigate uncertain parameters of rotating machines with constant speed of rotation subjected to a support motion. As the geometry of the skew disk is not well defined, randomness is introduced and affects the amplitude of the internal excitation in the time-variant equations of motion. This causes uncertainty in dynamical behavior, leading us to investigate its robustness. Stability un-der uncertainty is first studied by introducing a transformation of coordinates (feasible in this case) to make the problem simpler. Then, at a point far from the unstable area, the random forced steady state response is computed from the original equations of motion. An analytical method provides the probability of instability, whereas Taguchi's method is used to provide statistical moments of the forced response.

1 Introduction

The dynamical behavior of rotating machines has been thoroughly investigated [1,2]. It is well known that their complex dynamical behavior is mainly due to the rotating terms (gyroscopic effect) appearing in the equations of motion. When these machines are installed in a moving environment [2–4], the dynamical behavior exhibits certain typical parametrical phenomena (instability, quasiperiodic responses, etc.). Modeling a shaft-rotor system whose support is subjected to an imposed motion can be achieved by using numerical methods (finite elements) and semi-analytical methods (Rayleigh–Ritz) [3–5]. The equations of motion highlight nonclassical terms making resolution difficult: non-symmetrical matrices due to gyroscopic effects and parametric excitation [6] terms for a skew geometric shaft and /or for a rotating motion of the support [3,4].

Besides the problem of modeling dynamics, rotating machines are known to be very sensitive systems. This sensitivity considerably affects the vibratory behavior of slightly damped systems [7]. For many mechanical systems, the origin of this sensitivity can be traced to manufacturing dispersion. Designers try to avoid this variability by reducing all the tolerances of mounting and manufacturing processes. As a consequence, performances are guaranteed but production costs are still too high, making the product ill adapted to mass production. The tolerancing process leads to uncertainty in system geometry and thus uncertainty in overall behavior.

The above situation raises the question: Does this uncertainty harm performance? The problem of managing this uncertainty is currently investigated by using stochastic methods, Monte Carlo (MC) simulation, polynomial chaos, Taguchi's method [7,8], and analytical methods [9,10]. The efficiency of these techniques has been proven for linear mechanical systems [11], though little has been done in this field regarding the dynamical behavior of parametrically excited systems including gyroscopic terms.

The aim of this work is to apply stochastic methods to investigate uncertain parameters of rotating machines with constant speed of rotation subjected to a support motion. In this study, the equations of motion of a supported rotor equipped with an asymmetric disk are investigated. The support motion is a simple harmonic translation in one direction. The amplitude of parametric excitation, due to small changes in the system geometry, is considered as an uncertain parameter. As a consequence, the first issue to be considered concerns the uncertain stability problem. Stability is studied here by transforming the variables (from coordinates expressed in the fixed frame to coordinates expressed in the rotating frame), changing the parametric equation into a time invariant equation of motion. The computation of the natural frequencies of this new set of equations provides information on stability. It should be mentioned that this transformation of variables is always feasible even when the new set of equations of motion is not easier to solve than the original one. In particular when bearing stiffnesses are introduced in the fixed frame, they may be changed into parametrical terms. The probability of instability at a given speed of rotation is computed since it is possible to provide the probability density function (PDF) of the natural frequency. The probability density function is derived from the fundamental theorem on the function of one random variable.

In order to avoid numerical problems, we first ensure that all forced response computations are performed far from possibly unstable areas by computing the probability to be unstable. After guaranteeing the stability of the free response, further statistical results concerning the forced response near the primary and parametric resonances can be computed. Taguchi's method is used to provide the two first statistical moments of the forced responses and very good agreement with the results obtained using the Monte Carlo method is obtained.

2 Equations of Motion and Deterministic Behavior

2.1 Equations of Motion for Behavior in Bending. The rotor investigated is shown in Fig. 1. The equations of motion are

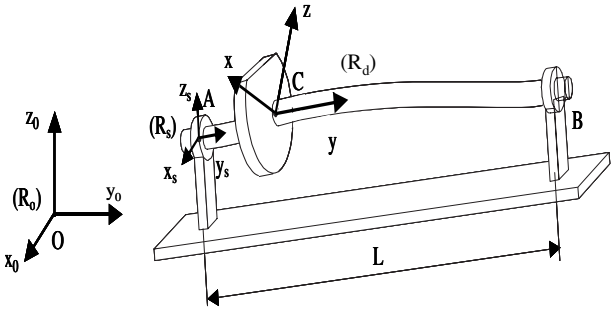

Fig. 1 View of the rotating machine model and associated frames

developed from the Rayleigh–Ritz method [1], and the derivation for bending deformations is completely described in Refs. [3–5]. The main steps of this derivation are as follows:

(i) choice of three different frames (R_d, frame moving with the disk; R_s, frame attached to the moving support; and R_0, frame fixed in space)
(ii) computation of the Lagrangian in the R_0 fixed frame
(iii) choice of an acceptable displacement shape function (Rayleigh method), and
(iv) use of Lagrange equations

Only the main assumptions used for this model are recalled here. The rotor is composed of a flexible shaft and a rigid disk. Asymmetrical geometry was chosen for the disk, a configuration often used in vacuum pumps. The shaft is in pinned-pinned configuration and the support is totally rigid. An imposed translational harmonic displacement is applied to the support in direction x_s, see Fig. 1. The speed of rotation Ω is assumed to be constant. An initial beam mode shape is considered here when applying the Rayleigh method. The general form of the equations of motion expressed in the R_s frame is

$$[\mathbf{M} + g(t)\mathbf{M_d} + h(t)\mathbf{M}_{\text{nd}}]\ddot{\mathbf{x}} + [\mathbf{C}_{\text{gyro+damp}} + g(t)\mathbf{C}_{\text{nd}} + h(t)\mathbf{C_d}]\dot{\mathbf{x}} + \mathbf{K}\mathbf{x} = \mathbf{f}(\mathbf{t}) \quad (1)$$

where

$$g(t) = I_{da}\cos(2\ \Omega t)$$

$$h(t) = I_{da}\sin(2\ \Omega t) \quad (2)$$

and

$$I_{da} = (I_{dxx} - I_{dzz})/2 \quad (3)$$

Equation (1) is a two degree of freedom (dof) matrix differential equation of the second order. It is a linear time-variant equation with periodic coefficients and gyroscopic terms. The parametric excitation (Eq. (2)) is due to the asymmetry geometry of the disk (I_{da} defined by Eq. (3)). The **x** vector describes the displacement of the middle point of the shaft in the R_s frame. The translational displacement of the base appears in the right hand side of Eq. (1) as an acceleration term. The external force vector can also include a residual mass unbalance (see Eq. (5)).

The rotor system has the following characteristics:

(i) The material is steel for the shaft and the disk.
(ii) The shaft has a length equal to $L = 0.4$ m with a circular cross section.
(iii) The disk is located at $L/3$.
(iv) Classical viscous damping is considered and is equal to $c = 2000$ N s m^{-1}.
(v) The mass unbalance is located on the disk and is equal to 8.66×10^{-6} kg m.

More detailed features are given in the Appendix. The imposed displacement is a harmonic cosine function with frequency ω_e and an amplitude of 0.1 cm in direction x_s (Fig. 1). Considering these characteristics and according to the formula given in Refs. [4,5], Eq. (1) expressed in standard units has the following numerical values:

$$\mathbf{M} = \begin{bmatrix} 13.5 & 0 \\ 0 & 13.5 \end{bmatrix}, \quad \mathbf{M_d} = \begin{bmatrix} -15.4 & 0 \\ 0 & 15.4 \end{bmatrix}$$

$$\mathbf{M}_{\text{nd}} = \begin{bmatrix} 0 & 15.4 \\ 15.4 & 0 \end{bmatrix}$$

$$\mathbf{C}_{\text{gyro+damp}} = \begin{bmatrix} 2000 & -2.4\ \Omega \\ 2.4\ \Omega & 2000 \end{bmatrix}$$

$$\mathbf{C_d} = \begin{bmatrix} 30.8\ \Omega & 0 \\ 0 & -30.8\ \Omega \end{bmatrix}, \quad \mathbf{C}_{\text{nd}} = \begin{bmatrix} 0 & 30.8\ \Omega \\ 30.8\ \Omega & 0 \end{bmatrix}$$

$$\mathbf{K} = \begin{bmatrix} 1.9e7 & 0 \\ 0 & 1.9e7 \end{bmatrix}, \quad \mathbf{x}(t) = \begin{Bmatrix} x(t) \\ z(t) \end{Bmatrix} \quad (4)$$

The rotor is subjected to a translational motion of the base, so the right hand side of Eq. (1) takes the following numerical values:

$$\mathbf{f}(t) = \begin{Bmatrix} 0.0144\omega_e^2\cos(\omega_e t) + 8.66 \times 10^{-6}\Omega^2\sin(\Omega t) \\ 8.66 \times 10^{-6}\Omega^2\cos(\Omega t) \end{Bmatrix} \quad (5)$$

To obtain the order of magnitude of the internal excitation, the numerical values of the disk inertia are the following:

$$I_{da} = 0.029\ \text{kg m}^2$$

$$I_{dm} = 0.077\ \text{kg m}^2 \quad (6)$$

where I_{dm} describes the inertia of symmetry of the disk. The following is a description of the deterministic dynamical behavior of the system employed and is given before introducing randomness in Eqs. (4) and (5) through the I_{da} parameter.

2.2 Deterministic Stability Analysis. Before computing the forced response, it is necessary to check the unstable areas according to the speed of rotation Ω and the amplitude of parametric excitation I_{da}. In our case the system of equations (4) could be easily transformed into a time invariant. As shall be seen, this transformation makes the resolution simpler, but this result cannot always be guaranteed for all time-variant systems. The stability analysis could have also been considered by using Floquet's theory. In this case, however the variables change from $\mathbf{x}(t)$ into $\mathbf{q}(t)$:

$$\mathbf{x}(t) = \begin{bmatrix} \cos(\Omega t) & \sin(\Omega t) \\ -\sin(\Omega t) & \cos(\Omega t) \end{bmatrix}\mathbf{q}(t) \quad (7)$$

This transformation leads to a new equation expressed in the rotating frame (R_d). It is as follows:

$$[\mathbf{M}_{\text{mob}}]\ddot{\mathbf{q}} + [\mathbf{C}_{\text{mob}}]\dot{\mathbf{q}} + [\mathbf{K}_{\text{mob}}]\mathbf{q} = \mathbf{f}_{\text{mob}}(t) \quad (8)$$

with the following numerical values:

$$\mathbf{M}_{\text{mob}} = \mathbf{M} + \begin{bmatrix} -15.4I_{da} & 0 \\ 0 & +15.4I_{da} \end{bmatrix}$$

$$\mathbf{C}_{\text{mob}} = \begin{bmatrix} 2000 & 24.6\ \Omega \\ -24.6\ \Omega & 2000 \end{bmatrix}$$

$$\mathbf{K}_{\text{mob}} = \mathbf{K} + \Omega\begin{bmatrix} -15.4I_{da}\Omega - 11.1\ \Omega & 2000 \\ -2000 & 15.4I_{da}\Omega - 11.1\ \Omega \end{bmatrix}$$

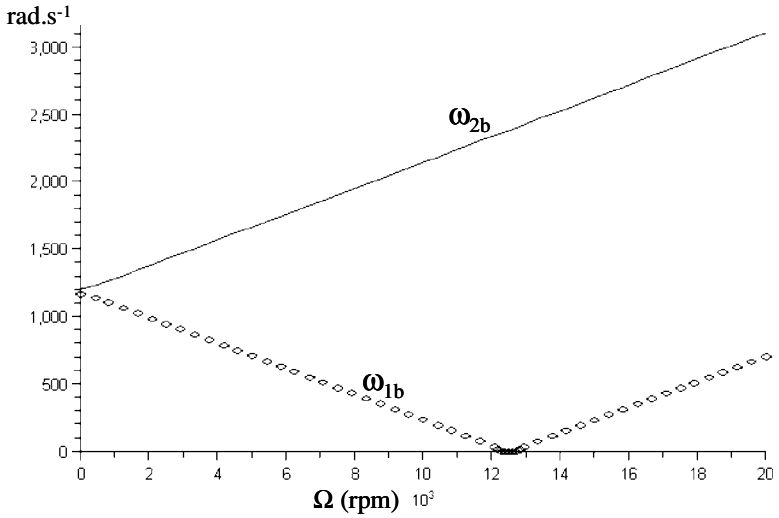

Fig. 2 Campbell diagram obtained in the rotating frame (R_d) for I_{da} = 0.029 kg m^2

$$\mathbf{f}_{\text{mob}}(t) = \begin{bmatrix} \cos(\Omega t) & -\sin(\Omega t) \\ \sin(\Omega t) & \cos(\Omega t) \end{bmatrix} \mathbf{f}(t) \tag{9}$$

The stability is then conducted by studying the eigenvalues of Eq. (8) with numerical expression (9), setting the right hand side as being equal to zero and neglecting the damping. The influence of the damping on the unstable boundaries is quite well known for parametrically excited systems. The damping does not change the frequencies where instabilities are found, but leads to an increase in the parametric excitation amplitude threshold. Neglecting the damping means that instabilities are more likely to occur. By taking the imaginary part of these eigenvalues, we obtain the two natural frequencies of the rotor, ω_{1b} and ω_{2b}. According to Ref. [12], when ω_{1b} is equal to zero the rotor is unstable, and the real part of the eigenvalue becomes positive. Figure 2 illustrates the two natural frequencies of the system studied according to the speed of rotation for I_{da} = 0.029 kg m^2. There is a narrow range within which the rotor is unstable, particularly at high speeds.

Other particular values of parameter I_{da} have been chosen and studied. The stability boundaries are summarized in Table 1. Inside the Ω-ranges given in Table 1, the rotating machine is unstable while it is stable outside them. Regarding the influence of I_{da} on the unstable ranges, we can conclude that the sensitivity of the rotor is very low.

2.3 Deterministic Forced Response. In our case, the computation of the forced response could have been conducted by using Eq. (8) with the values given by Eq. (9). This method is not the most general for all kinds of rotating machines. This is why we prefer studying the problem starting from its original set of equations (1).

As there is no analytical solution for Eq. (1), a numerical scheme is used to provide stable forced responses. In this field, the main numerical method used is the Newmark scheme in the time domain. Unfortunately this integration process is very time consuming when the system is subjected to a wide frequency band excitation (Ω and ω_e could be considerably different) and does not take advantage of the periodic nature of the time-variant coefficients. This leads us to adapt an original numerical scheme proposed and described in Ref. [13] to our case. This original method works in the spectral domain and requires less computational time as it takes advantage of the periodic nature of the parametric terms. The method was first devoted to parametric linear systems with a time-variant periodic stiffness. The addition of gyroscopic terms and other time-variant coefficients does not change the method of implementing the spectral method [14]. The spectral process is divided into the following three steps:

(i) decoupling the equations of motion (Eq. (1)) by expanding it, using the modal time-average basis
(ii) taking the Fourier transform of the pseudomodal system obtained in (i), and finally
(iii) solving the equations by a fixed point algorithm

To prove the efficiency of this method, Fig. 3 shows an example of the forced responses obtained with both Newmark and spectral methods. The running parameters are ω_e = 15.9 Hz and Ω = 2000 rpm (almost 33.2 Hz). The main differences between both forced responses are observed for the *z* displacement forced response. According to Eqs. (4) and (5), the spectra of each dof could be composed by ω_e, Ω, 2 Ω ± ω_e, 2 Ω ± Ω, etc. The *x* forced response is mainly composed of the ω_e component, explained by the fact that the base excitation is much greater than the excitation due to the mass unbalance. The *z* forced response is composed of ω_e, Ω, and 2 Ω ± ω_e. Finally, the comparison reveals good agreement between both methods with a computational time divided by 100.

Other deterministic results could be easily obtained with different running conditions. Figure 4 shows the spectrum of both dofs for Ω = 166.2 Hz and ω_e = 15.8 Hz. The excitation amplitudes remain the same as those of the previous case except (as the speed of rotation has increased) the mass unbalance excitation, which is greater. The frequency content of the *x* forced response becomes more complex. It is now possible to give more results for the deterministic dynamical behavior of the device studied.

As Eq. (1) is a linear time-variant equation, there is no natural frequency in the "classical" sense. Fortunately, we are still able to derive a Campbell diagram derived from that plotted in Fig. 2: It is simply necessary to add term ±Ω to the natural frequencies obtained in R_d. The Campbell diagram derived is shown in Fig. 5.

Table 1 Unstable speed of rotation ranges for particular values of I_{da}

I_{da} (kg m^2)	Ω min (rpm)	Ω max (rpm)
0.0261	12,275	12,725
0.0290	12,250	12,755
0.0319	12,230	12,780

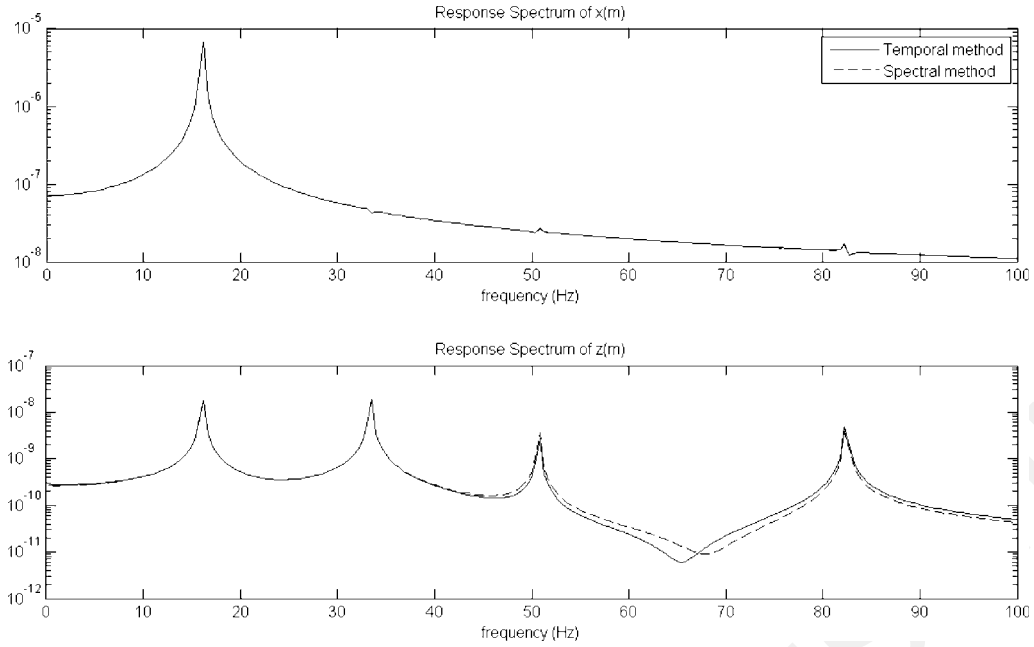

Fig. 3 Comparison between the spectra of *x* and *z* forced responses provided by a Newmark scheme and the spectral method; Ω=33.2 Hz and ω_e=15.8 Hz

Let us now focus on the forced steady state response. Figure 6 displays the rms resonant curve for the *x* displacement. The resonantly excited natural frequencies are $\omega_e \approx \omega_1 = \omega_{2b} - \Omega$ and $\omega_e \approx \omega_2 = \omega_{1b} + \Omega$. As these frequencies are very close at low speeds of rotation, only a single main peak is observed. For *x* dof, the base excitation dominates the mass unbalance excitation.

Figure 7 displays the rms forced response of the *z* displacement. Secondary resonant peaks appear at low speeds of rotation for frequencies, respectively, equal to $\omega_4 = \omega_{2b} + \Omega$ and $\omega_3 = \omega_{1b} - \Omega$. They are due to parametric resonances. For this dof, the main resonant response is due to an excitation of the forward mode by the mass unbalance.

3 Description of Stochastic Methods Used

3.1 Monte Carlo Simulation. Monte Carlo simulations are commonly used to obtain reference predictions in order to test other statistical methods. Monte Carlo simulation requires a large number of samples, therefore significantly increasing processing time since computations of forced responses must be performed and stored for each sample. The statistical moments PDFs are deduced at the end of the simulation. The accuracy and the number of samples required greatly depend on the random number generator. In order to generate Gaussian variables, a Box and Muller algorithm is used here to transform a uniform distribution

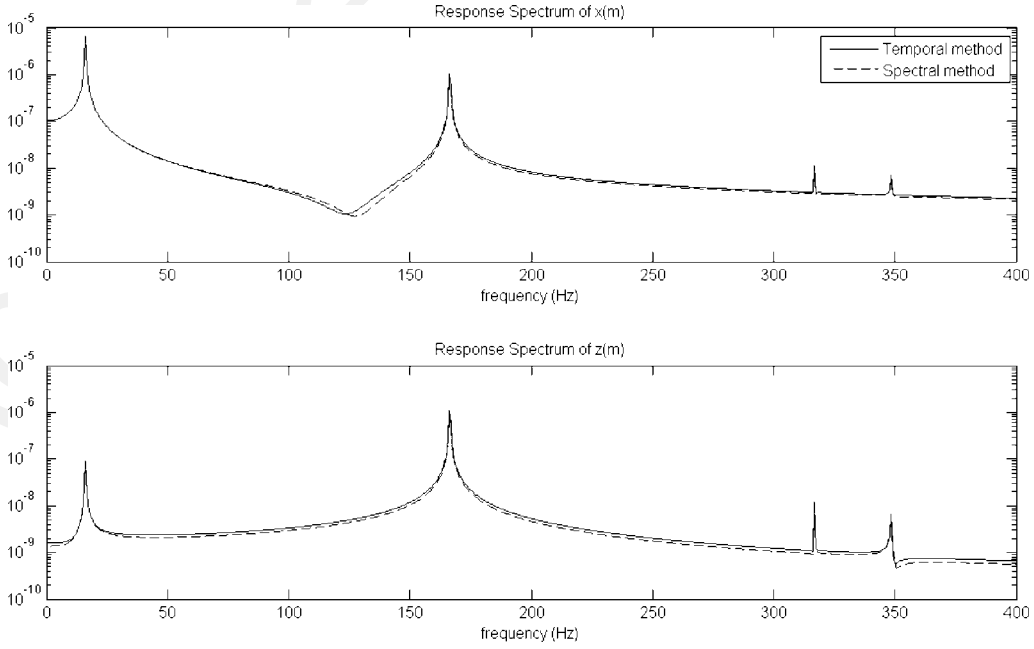

Fig. 4 Comparison between the spectra of *x* and *z* forced responses provided by a Newmark scheme and the spectral method; Ω=166.2 Hz and ω_e=15.8 Hz

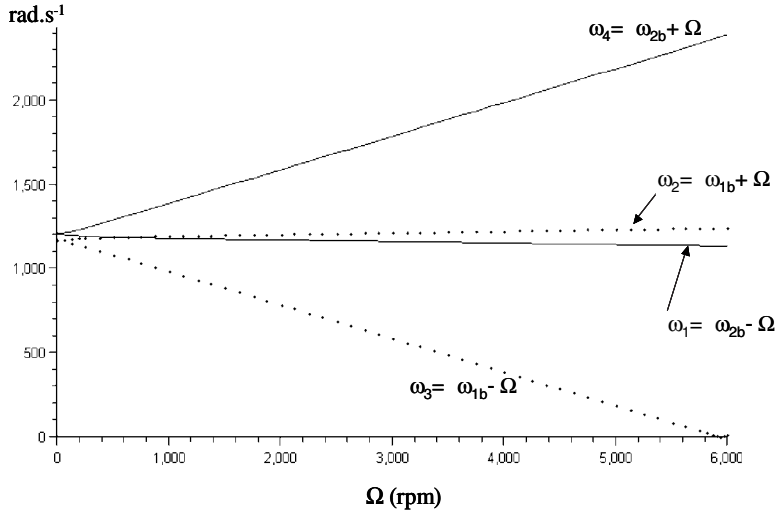

Fig. 5 Campbell diagram obtained in the fixed frame

between 0 and 1 into a Gaussian distribution with a chosen mean value and standard deviation. As the convergence rate of this process is proportional to function $1/\sqrt{n}$, the number of samples chosen is at least equal to 10,000.

3.2 Taguchi's Method. Taguchi's method allows very simple estimation of the statistical moments of a function of multiple random variables whose PDFs are known [15]. This method has been improved by D'Errico and Zaino [16], in order to take into account nonlinear response effects, and a modified Taguchi method has been used for heat processing problems [17]. The theoretical expressions for the first two moments of a function $f(\mathbf{x})$ of k randomly independent variables ${}^t\mathbf{x}=\langle x_1,\ldots,x_k\rangle$ are

$$E[f(\mathbf{x})] = \int_{-\infty}^{+\infty} f(\mathbf{x}) p_1(x_1)\cdots p_k(x_k)dx_1\cdots dx_k \qquad (10)$$

$$\mathrm{var}[f(\mathbf{x})] = \int_{-\infty}^{+\infty} (f(\mathbf{x}) - E[f(\mathbf{x})])^2 p_1(x_1)\cdots p_k(x_k)dx_1\cdots dx_k \qquad (11)$$

In D'Errico's method, each PDF of a given random variable is sampled at three or more points and a weighting coefficient is assigned to each point depending on its PDF type. For example, Fig. 8 gives the three point discretization of a random Gaussian (μ_i is the mean value, s_i is the standard deviation) with associated weightings w_i. The response function is evaluated for all point combinations and is equivalent to a full factorial design of experiments with M responses and point combinations. The modified Taguchi process is based on numerical integration techniques such as the Gauss–Hermite quadrature method for the function of multiple variables. The mean value and the variance of the function are estimated by a linear combination of the responses obtained

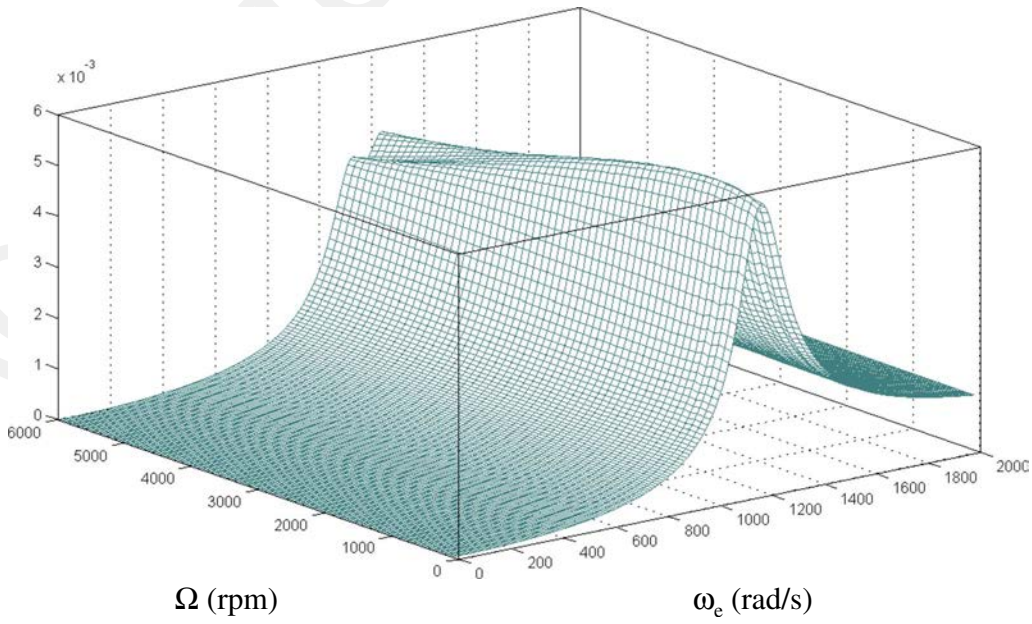

Fig. 6 rms value of the *x* displacement (*m*) response versus Ω and ω_e

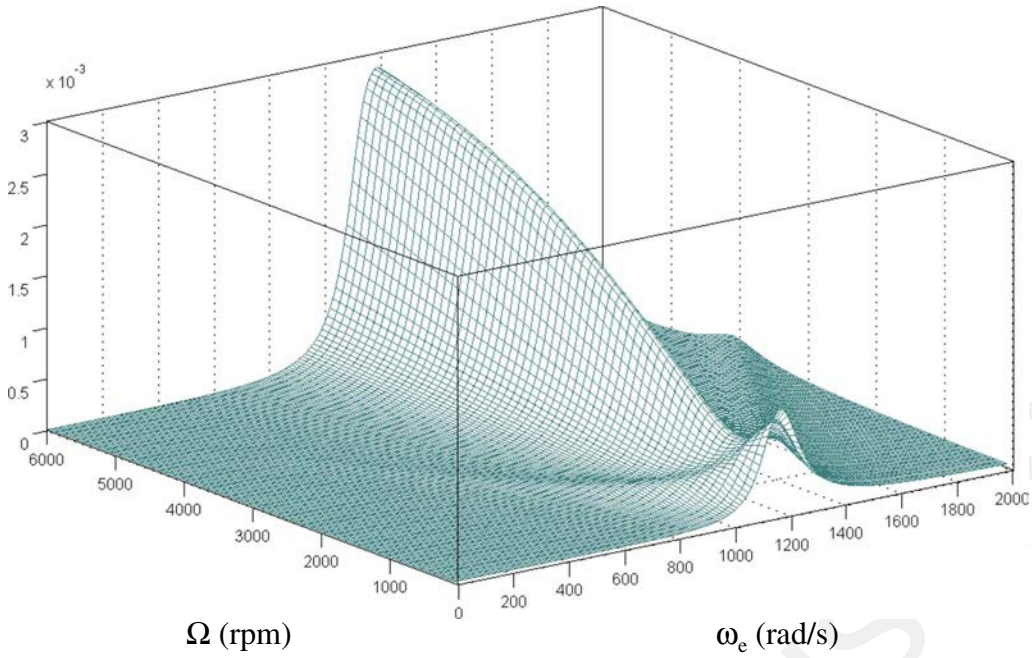

Fig. 7 rms value of the *z* displacement response (*m*) versus Ω and ω_e

previously with the full factorial design of experiments as follows:

$$E[f(\mathbf{x})] = \sum_{i=1}^{M} W_i f_i \tag{12}$$

$$\mathrm{var}[f(\mathbf{x})] = \sum_{i=1}^{M} W_i (f_i - E[f(\mathbf{x})])^2 \tag{13}$$

where $W_i = \Pi_{i=1}^{k} w_i$. For each uncertain variable, at least three samples are necessary to take into account the nonlinear behavior of the response function. Accuracy increases rapidly with the number of samples considered. The main advantages of this method are its easy numerical implementation and its computational efficiency. Furthermore, non-Gaussian PDFs can be easily introduced by choosing convenient points and weightings. Regarding this, see, for example, Ref. [18]. Taguchi's method is a nonintrusive technique compared with expansion techniques (Taylor, perturbation, etc.). However, Taguchi's method cannot provide the PDF of the response function, which can be considered as a disadvantage.

4 Uncertain Dynamical Behavior

This step entails the investigation of the uncertain dynamical behavior of the rotating machine described previously. The uncertain random parameter is chosen as I_{da}. The random nature of I_{da} could be a topic of discussion on its own. Our aim is to prove the efficiency of Taguchi's method and also to investigate possible differences between the deterministic and random behaviors of the rotor. I_{da} is now considered as a Gaussian parameter with a mean value equal to 0.029 kg m^2 and a standard deviation equal to 10% of the mean value.

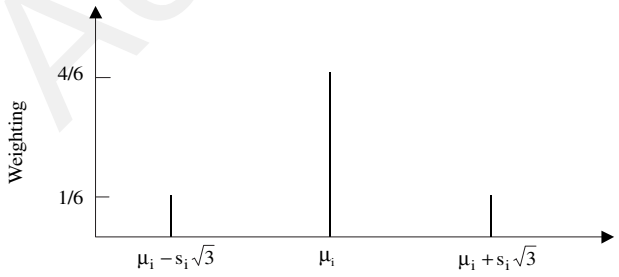

Fig. 8 Points and weightings for a three point-sampled Gaussian variable

4.1 Stability Under Uncertainty: Analytical Method. Designers need to obtain a reliable estimation of the probability P_Ω of instability for a given speed of rotation Ω. The unstable feature of the motion is found when the real part of one of the eigenvalues of Eq. (8) (numerical values given by Eq. (9), right hand side set to zero, and damping neglected) becomes strictly positive. As the eigenvalues depend on I_{da} and Ω, they also have a random nature. Consequently, P_Ω requires the computation of the PDF of the eigenvalue, which may have a positive real part. Let λ be the real part of this eigenvalue and let $h_\Omega(x)$ be its PDF, then the theory of probability leads to

$$P_\Omega = 100 \times \int_{0^+}^{+\infty} h_\Omega(\lambda) d\lambda \tag{14}$$

According to Papoulis [10], $h_\Omega(\lambda)$ could be computed through an analytical process. Let

$$\lambda = g(I_{da}, \Omega) \tag{15}$$

be the map linking λ and I_{da}. In our case, I_{da} is physically bounded as $0 < I_{da} < 0.1$. Consequently, we restrict our derivation to this interval.

The analytical process discussed by Papoulis is only applicable for a certain class of maps. Now let us examine the behavior of Eq. (15). Figure 9(*a*) plots Eq. (15) for Ω = 12,250 rpm. This function is null until I_{da} reaches a threshold I_{da}^t. After this threshold, Eq. (15) is a one-to-one mapping such that the fundamental theorem [10] works simply, giving

$$h_\Omega(\lambda) = \sum_i \frac{p(x_i)}{|g'(x_i)|} \quad \text{where } g' = \frac{dg}{dx} \tag{16}$$

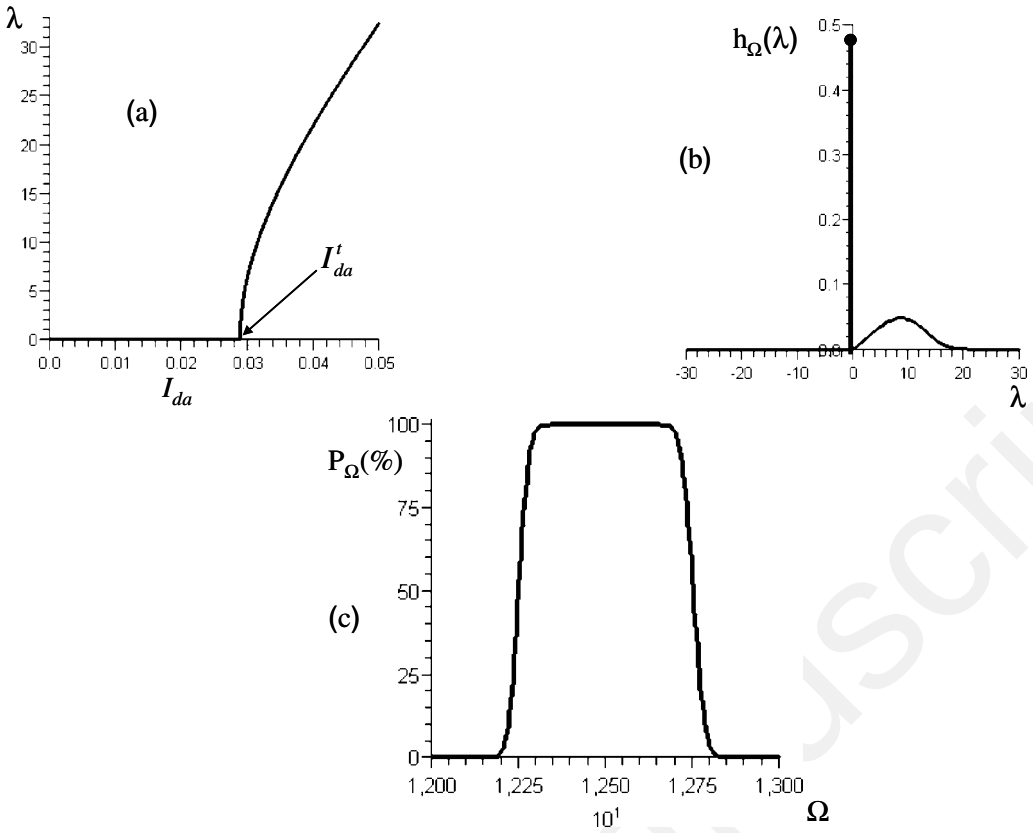

Fig. 9 $g(I_{da}, \Omega = 12{,}250)$ (*a*), **PDF** $h_\Omega(\lambda)$ **computed at** $\Omega = 12{,}250$ **rpm** (*b*), **and probability** P_Ω **to be unstable** (*c*)

where $p(x)$ is the PDF of I_{da}, and x_i are the real roots of Eq. (15).

Before this threshold, Eq. (15) is null and has an infinite number of real solutions. Consequently $h_\Omega(\lambda)$ contains an impulse function at the origin of area A given by

$$A = \int_{-\infty}^{I^t_{da}} p(x)dx \cong \int_{0}^{I^t_{da}} p(x)dx \tag{17}$$

Moreover, by assumption

$$\lambda \geq 0 \tag{18}$$

then

$$h_\Omega(\lambda) = 0 \quad \text{for} \quad \lambda \in \;]-\infty \cdots 0[\tag{19}$$

But recalling that $p(x)$ is a Gaussian PDF, we are able to compute $h_\Omega(\lambda)$ for all the values of speed of rotation Ω. Figure 9(*b*) shows $h_\Omega(\lambda)$ for $\Omega = 12{,}250$ rpm. The impulse function is of great importance even if it is not taken into account in formula (14). It ensures that the full integration of the PDF is equal to 1. The impulse function vanishes for $\Omega = 12{,}600$ rpm. Figure 9(*c*) displays the probability of instability versus the speed of rotation. The speed ranges given in Table 1 are in good agreement with the probability obtained here. The analytical process is not always so easy to implement. Each case must be considered with care depending on the nature of the relation (Eq. (15)).

4.2 Uncertain Steady State Response: Taguchi's Method. We now focus on the uncertain forced response. The implementation of the analytical process described earlier is not feasible here, so Taguchi's is used. Figure 10 shows the mean value and the standard deviation of the *x* rms displacement, while the running condition is $\Omega = 1000$ rpm. The Monte Carlo simulation was achieved using 10,000 samples, whereas Taguchi's method required only three samples. Compared with the deterministic results (Fig. 6) the orders of magnitude of the predicted mean values are the same. The mean value seems to be quite close to the deterministic response. In contrast, the standard deviation exhibits more troubled behavior. In order to obtain an order of magnitude of the maximum values that could be reached by the response, the Chebyshev inequality can be used. This would result in a maximum frequency response curve, highlighting two resonant frequencies that differ from the deterministic one. This fact is perhaps one of the most important results in the field of uncertain dynamical systems. Finally, Taguchi's method agrees very well with the Monte Carlo method.

The comments are the same for the other forced responses obtained under different running conditions (see Fig. 11). Moreover, as the standard deviation is 100 times less than the mean value, it can be concluded that the introduction of randomness in parameter I_{da} does not greatly affect the dynamics of this rotor machine. This conclusion is very interesting because the input dispersion is not negligible.

The comparison between Fig. 12 (mean values of the forced response) and Fig. 7 (deterministic forced response) confirms this fact. The sensitivity of the system to asymmetry inertia is quite low. The disk does not require a high precision manufacturing process.

Finally, as Taguchi's method reveals itself to be a very efficient tool for computing the statistical moments of the forced response, Fig. 13 illustrates the standard deviation of the *z* rms displacement response. As can be observed, the main output dispersion is located on secondary resonances and for low speed of rotation values. Indeed, the randomness of parameter I_{da} appears to play a major role when the system response is not too high.

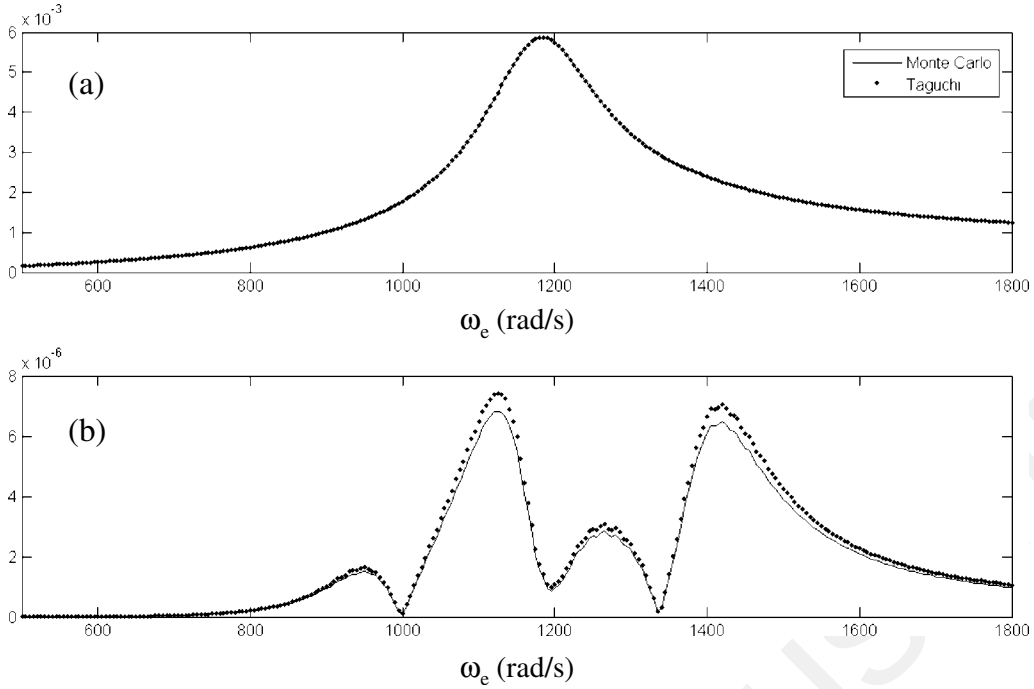

Fig. 10 Mean value (*a*) and standard deviation (*b*) of the rms forced response (*m*) versus ω_e in the *x* direction provided by MC and Taguchi's methods; Ω=1000 rpm

5 Conclusion

This study achieved two goals. The first was to show that the introduction of stochastic parameters is one way to obtain more information on the sensitivity of a rotating machine. The uncertain stability analysis was investigated by using an analytical process not considered to be the most general tool. Indeed, certain essential mathematical properties are usually missing, so that the Monte Carlo simulation is the only method of building the PDF of a function of one random variable. The case studied here provides interesting information, making it possible to quantify the robustness of stability with great accuracy.

Regarding the forced response, the use of Taguchi's method does not require cumbersome mathematical developments such as those required for classical sensitivity analysis (for example, the

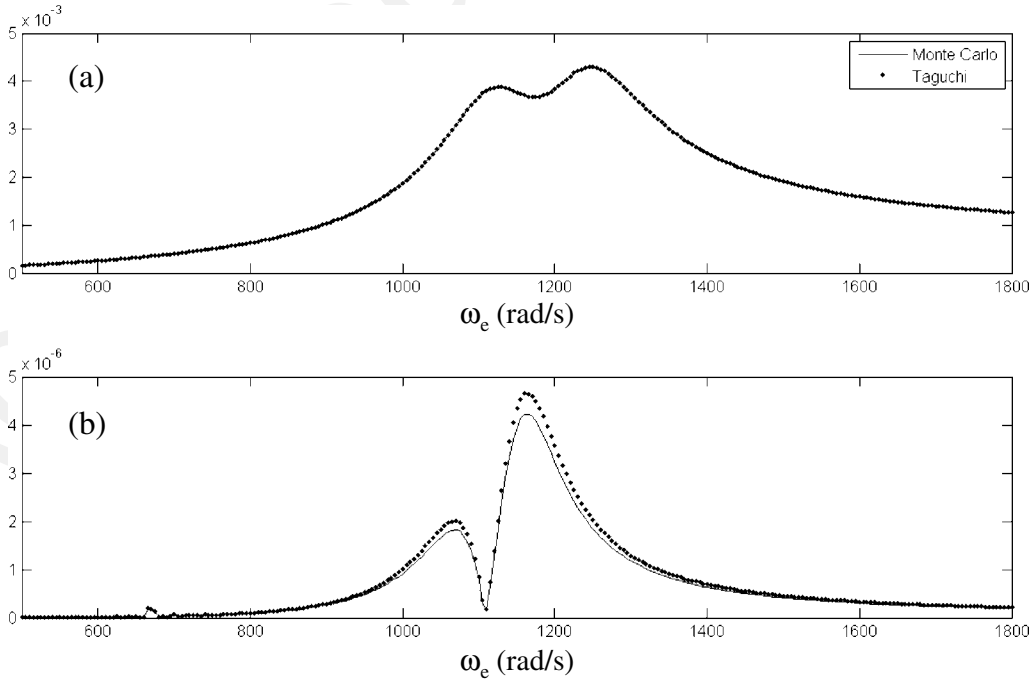

Fig. 11 Mean value (*a*) and standard deviation (*b*) of the rms forced response (*m*) versus ω_e in the *x* direction provided by MC and Taguchi's methods; Ω=6400 rpm

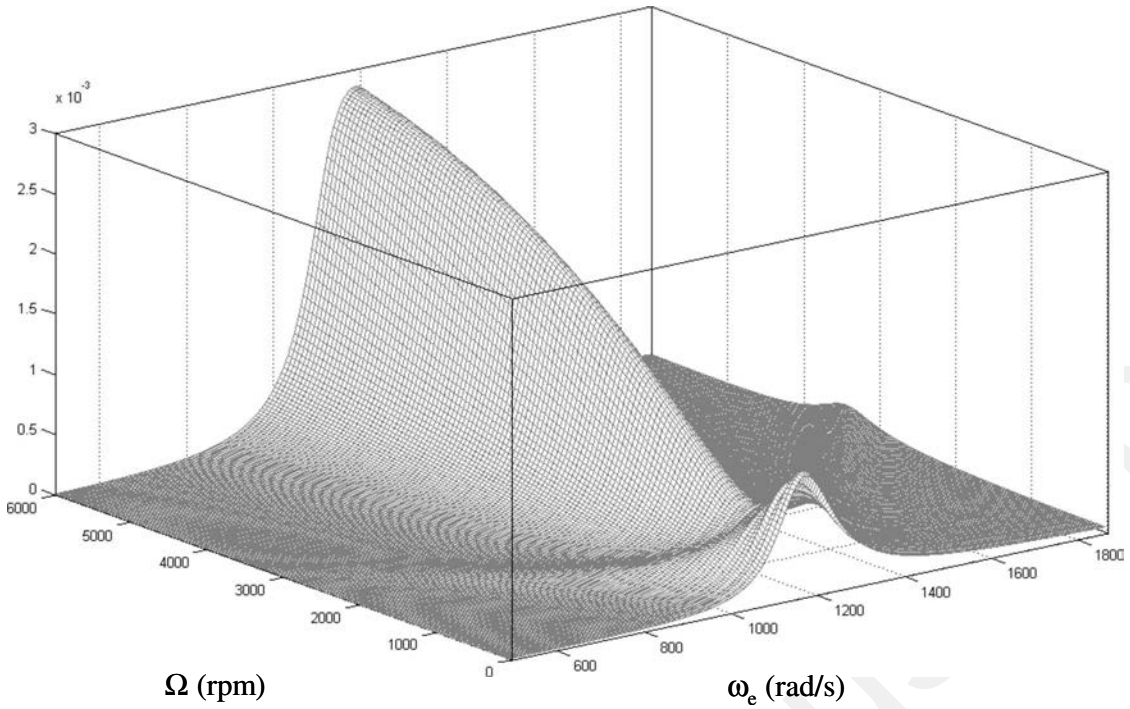

Fig. 12 Mean values of the *z* rms forced response (*m*) versus Ω and ω_e provided by Taguchi's method

computation of partial derivatives). The first statistical moments can be used easily to obtain the bounded values reached by the machine in operation. The second goal was to obtain useful information on the random nature of the dynamical parametric behavior. As the output variability is not high in this case, it is impossible to extrapolate a trend from these results. The rotating machine seems to be robust with respect to the parametric excitation. The work must be extended in other directions, for example, considering the overall dynamics, not only those close to the first critical speeds, analyzing nonlinear behavior due to shaft bearing clearance asymmetry, etc. Another interesting path for development is to consider accelerating rotors [2,3] (Ω speed fluctuations) subjected to a steady state ground motion, as the transient nature of this particular motion makes the application of the spectral method unfeasible.

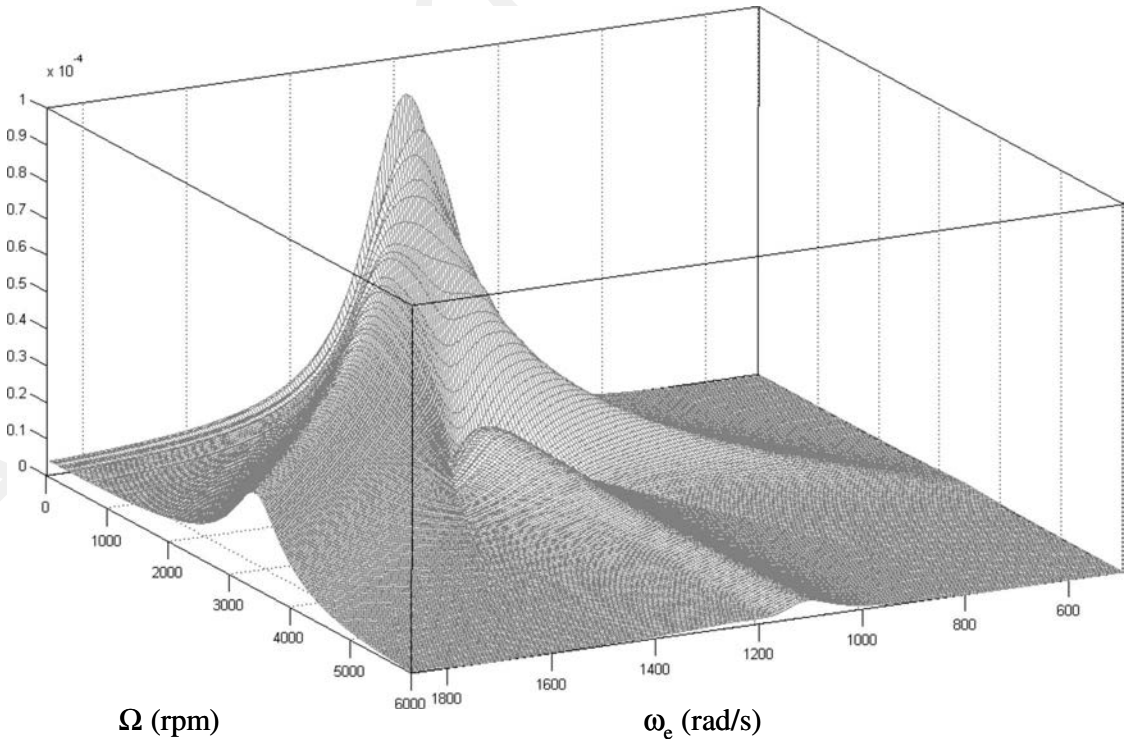

Fig. 13 Standard deviation of the *z* rms displacement (*m*) versus Ω and ω_e by Taguchi's method

Table 2 Features of the rotor

Shaft	
Length of the shaft L	0.4 m
Mass density ρ	7800 kg m^{-3}
Young modulus E	2.11×10^{11} Pa
Poisson's ratio ν	0.3
Radius of cross section r	0.02 m
Mass unbalance	
m_u	10^{-4} kg
Distance from the axis of rotation d	0.1 m
Disk	
Thickness e	0.03 m
Mass density ρ	7800 kg m^{-3}
Young modulus E	2.11×10^{11} Pa
Poisson's ratio ν	0.3
Mass	14 kg
Radius	0.138 m

Appendix

Table 2 provides the main feature of the studied rotor.

References

[1] Lalanne, M., and Ferraris, G., 1998, *Rotordynamics Predictions in Engineering*, 2nd ed., Wiley, New York.

[2] Rao, J. S., 1991, *Rotor Dynamics*, 2nd ed., Wiley, New York.

[3] Krämer, E., 1993, *Dynamics of Rotors and Foundations*, Springer-Verlag, New York.

[4] Duchemin, M., Berlioz, A., and Ferraris, G., 2006, "Dynamic Behavior and Stability of a Rotor Under Base Excitation," ASME J. Vibr. Acoust., **128**(5), pp. 576–585.

[5] Driot, N., Lamarque, C. H., and Berlioz, A., 2006, "Theoretical and Experimental Analysis of a Base Excited Rotor," ASME J. Comput. Nonlinear Dyn., **1**(3), pp. 257–263.

[6] Tondl, A., 1992, "Parametric Resonance Vibration in a Rotor System," Acta Tech. CSAV, **37**, pp. 185–194.

[7] Mace, B. R., Worden, K., and Manson, G., eds., 2005, "Uncertainty in Structural Dynamics," J. Sound Vib., **288**(3), pp. 423–790, special issue.

[8] Driot, N., and Perret-Liaudet, J., 2006, "Variability of Modal Behavior in Terms of Critical Speeds of a Gear Pair Due to Manufacturing Errors and Shaft Misalignments," J. Sound Vib., **292**, pp. 824–843.

[9] Heinkelé, C., Pernot, S., Sgard, F., and Lamarque, C. H., 2006, "Vibration of an Oscillator With Random Damping: Analytical Expression for the Probability Density Function," J. Sound Vib., **296**(1–2), pp. 383–400.

[10] A. Papoulis, 1965, *Probability, Random Variables and Stochastic Processes* (McGraw-Hill Series in Systems Science), McGraw-Hill, New York.

[11] Ibrahim, R. A., 1987, "Structural Dynamics With Parameter Uncertainties," Appl. Mech. Rev., **40**(3), pp. 309–328.

[12] Muszynska, A., 2005, *Rotordynamics*, CRC, Boca Raton, FL/Taylor and Francis, London.

[13] Perret-Liaudet, J., 1996, "An Original Method for Computing the Response of a Parametrically Excited Forced System," J. Sound Vib., **196**(2), pp. 165–177.

[14] Bachelet, L., Driot, N., and Ferraris, G., 2006, "Rotors Under Seismic Excitation: A Spectral Approach," *Proceedings of the IFToMM Seventh International Conference on Rotor Dynamics*, Vienna, Austria, Sept. 25–28.

[15] Taguchi, G., 1978, "Performance Analysis Design," Int. J. Prod. Res., **16**(6), pp. 521–530.

[16] D'Errico, J. R., and Zaino, N. A., 1988, "Statistical Tolerancing Using a Modification of Taguchi's Method," Technometrics, **30**(4), pp. 397–405.

[17] Yu, J. C., and Ishii, K., 1993, "A Robust Optimization Procedure for Systems With Significant Non-Linear Effects," ASME Design Automation Conference, Vol. DE-65-1, pp. 371–378.

[18] Abramowitz, M., and Stegun, I. A., 1972, *Handbook of Mathematical Functions*, Dover, New York.